

## Covalent Functionalization and Electron-Transfer Properties of Vertically Aligned Carbon Nanofibers: The Importance of Edge-Plane Sites

Elizabeth C. Landis,<sup>†</sup> Kate L. Klein,<sup>‡,§</sup> Albert Liao,<sup>||</sup> Eric Pop,<sup>||</sup> Dale K. Hensley,<sup>§</sup> Anatoli V. Melechko,<sup>§,⊥</sup> and Robert J. Hamers<sup>\*,†</sup>

<sup>†</sup>Department of Chemistry, University of Wisconsin–Madison, 1101 University Avenue, Madison, Wisconsin 53706, <sup>‡</sup>Department of Materials Science and Engineering, University of Tennessee, Knoxville, Tennessee 37996, <sup>§</sup>Center for Nanophase Materials Sciences Division, Oak Ridge National Laboratory, Oak Ridge, Tennessee 37831, <sup>||</sup>Department of Electrical and Computer Engineering, Micro and Nanotechnology Laboratory, University of Illinois at Urbana–Champaign, Urbana, Illinois 61801, and <sup>⊥</sup>Materials Science and Engineering Department, North Carolina State University, Raleigh, North Carolina 27695

Received November 30, 2009. Revised Manuscript Received January 18, 2010

The use of covalently bonded molecular layers provides a way to combine the outstanding stability and electrochemical properties of carbon-based structures with the unique properties of molecular structures for applications such as electrocatalysis and solar conversion. The functionalization of vertically aligned carbon nanofibers (VACNFs) with 1-alkenes, using ultraviolet light, was investigated as a potential way to impart a variety of different functional groups onto the nanofiber sidewalls. We report how variations in the nanofiber growth rate impact both the amount of exposed edge-plane sites and the resulting electrochemical activity toward  $\text{Ru}(\text{NH}_3)_6^{3+/2+}$  and  $\text{Fe}(\text{CN})_6^{3-/4-}$  redox couples. Measurements of the distribution of surface oxides show that surface oxides are unaffected by the grafting of alkenes to the nanofibers. Carbon nanofiber reactivity was also compared to multiwalled and single-walled carbon nanotubes. Our results demonstrate that edge-plane sites are preferred sites for photochemical grafting, but that the grafting of molecular layers only slightly reduces the overall electrochemical activity of the nanofibers toward the  $\text{Ru}(\text{NH}_3)_6^{3+/2+}$  couple. These results provide new insights into the relationships between the chemical reactivity and electrochemical properties of nanostructured carbon materials and highlight the crucial role that exposed edge-plane sites play in the electrochemical properties of carbon nanotubes and nanofibers.

### Introduction

There has been increasing interest in nanoscale carbon materials because of their high stability, surface area, and electrical conductivity.<sup>1–3</sup> The utility of carbon nanomaterials, in principle, can be further increased by covalently linking molecules that will confer specific properties (e.g., chemical selectivity, catalytic behavior, or molecular recognition properties) to the materials. The resulting properties are potentially of high importance for a range

of applications including electroanalysis,<sup>4,5</sup> sensing,<sup>6–10</sup> energy storage,<sup>11,12</sup> and electrocatalysis.<sup>13</sup> Previous studies have shown that the edge-plane sites play extremely important roles in the chemical properties of carbon-based materials,<sup>14–16</sup> and electron-transfer rates at edge-plane graphite are reported to be  $\sim 10^5$  times higher than those at basal-plane graphite.<sup>17</sup> Consequently, the number density of exposed graphitic edge planes is often

\*Author to whom correspondence should be addressed. Tel.: (608)262-6371. E-mail: rjhamers@wisc.edu.

- (1) Baughman, R. H.; Zakhidov, A. A.; de Heer, W. A. *Science* **2002**, *297*, 787.
- (2) Melechko, A. V.; Klein, K. L.; Fowlkes, J. D.; Hensley, D. K.; Merkulov, I. A.; McKnight, T. E.; Rack, P. D.; Horton, J. A.; Simpson, M. L. *J. Appl. Phys.* **2007**, *102*.
- (3) Melechko, A. V.; Merkulov, V. I.; McKnight, T. E.; Guillorn, M. A.; Klein, K. L.; Lowndes, D. H.; Simpson, M. L. *J. Appl. Phys.* **2005**, *97*.
- (4) McKnight, T. E.; Melechko, A. V.; Fletcher, B. L.; Jones, S. W.; Hensley, D. K.; Peckys, D. B.; Griffin, G. D.; Simpson, M. L.; Ericson, M. N. *J. Phys. Chem. B* **2006**, *110*, 15317.
- (5) McKnight, T. E.; Melechko, A. V.; Austin, D. W.; Sims, T.; Guillorn, M. A.; Simpson, M. L. *J. Phys. Chem. B* **2004**, *108*, 7115.
- (6) Lee, C. S.; Baker, S. E.; Marcus, M. S.; Yang, W. S.; Eriksson, M. A.; Hamers, R. J. *Nano Lett.* **2004**, *4*, 1713.

- (7) Baker, S. E.; Colavita, P. E.; Tse, K. Y.; Hamers, R. J. *Chem. Mater.* **2006**, *18*, 4415.
- (8) Baker, S. E.; Tse, K. Y.; Hindin, E.; Nichols, B. M.; Clare, T. L.; Hamers, R. J. *Chem. Mater.* **2005**, *17*, 4971.
- (9) Baker, S. E.; Tse, K. Y.; Lee, C. S.; Hamers, R. J. *Diamond Relat. Mater.* **2006**, *15*, 433.
- (10) Fletcher, B. L.; McKnight, T. E.; Melechko, A. V.; Simpson, M. L.; Doktycz, M. J. *Nanotechnology* **2006**, *17*, 2032.
- (11) Frackowiak, E.; Beguin, F. *Carbon* **2001**, *39*, 937.
- (12) Tse, K. Y.; Zhang, L.; Baker, S. E.; Nichols, B. M.; West, R.; Hamers, R. J. *Chem. Mater.* **2007**, *19*, 5734.
- (13) Kim, C.; Kim, Y. J.; Kim, Y. A.; Yanagisawa, T.; Park, K. C.; Endo, M.; Dresselhaus, M. S. *J. Appl. Phys.* **2004**, *96*, 5903.
- (14) Banks, C. E.; Davies, T. J.; Wildgoose, G. G.; Compton, R. G. *Chem. Commun.* **2005**, 829.
- (15) Banks, C. E.; Compton, R. G. *Analyst* **2005**, *130*, 1232.
- (16) Banks, C. E.; Ji, X. B.; Crossley, A.; Compton, R. G. *Electroanalysis* **2006**, *18*, 2137.
- (17) Rice, R. J.; McCreery, R. L. *Anal. Chem.* **1989**, *61*, 1637.

considered a key parameter controlling the electrochemical behavior of carbon-based materials.<sup>14–21</sup>

Vertically aligned carbon nanofibers (VACNFs) are a particularly interesting form of carbon, because, unlike carbon nanotubes, the molecular structure of VACNFs consists of stacked cones of graphite that expose large amounts of edge-plane graphite along their sidewalls.<sup>3,22,23</sup> Furthermore, each nanofiber has a direct electrical contact to the substrate. Recent studies have shown that varying the growth conditions can alter the angle at which the VACNF graphene cones intersect the nanofiber edge, thereby leading to the ability to tune the relative amounts of edge-plane and basal-plane graphite that is exposed.<sup>2</sup> This enables the ability to investigate the role of edge planes in controlling the chemistry and electrical properties of this unique form of nanostructured carbon.

Photochemical grafting of terminal alkenes has recently emerged as a method for grafting molecules to carbon surfaces such as diamond,<sup>24,25</sup> amorphous carbon,<sup>26,27</sup> glassy carbon,<sup>8,28</sup> and VACNFs.<sup>7,9,29,30</sup> With regard to VACNFs, this method has been used to attach and detect redox activity of molecules such as Cytochrome c to the nanofiber sidewalls.<sup>7,8,29</sup> Studies on diamond and amorphous carbon have shown that photochemical grafting is initiated by the photoemission of electrons from the substrate into adjacent reactive liquid.<sup>25,27,31</sup> As a result, the electronic structure of the carbon and the electron acceptor levels of the alkenes impact the reaction efficiency on the surfaces. However, previous studies have not identified whether edge vs basal planes affect photochemical grafting, nor have they established how the bonding of molecular substituents impacts the electrochemical properties of the nanofibers.

Here, we present studies aimed at understanding the interplay between nanoscale structure, photochemical grafting efficiency, and electrochemical properties of VACNFs. Our results show that the electrochemical activity and the photochemical reactivity of VACNFs are both dependent on the density of exposed edge planes and can be controlled by modifying the nanofiber growth

conditions. Using redox species to probe the density of exposed edge planes and basal planes, we demonstrate that the photochemical reaction leads to preferential grafting of molecules to the edge-plane sites of the vertically aligned carbon nanofibers, but that the electrochemical activity of the basal planes is essentially unchanged. By chemically derivatizing reactive oxygen groups such as alcohols, carboxylic acid, and carbonyl groups,<sup>32–34</sup> and characterizing their distribution before and after grafting, we show that nascent oxidized sites do not significantly impact the photochemical grafting. Most importantly, our results show that although the molecular substituents preferentially bind to the exposed edge-plane sites, the resulting nanofibers retain their electrochemical activity toward redox-active species such as  $\text{Ru}(\text{NH}_3)_6^{3+/2+}$ .

## Experimental Section

**Carbon Nanostructure Growth.** VACNFs were grown by plasma-enhanced vapor deposition (PECVD)<sup>8</sup> in two similar growth systems. Nanofibers were grown on silicon wafers, using a nickel catalyst deposited directly onto the silicon substrate or, in some cases, onto films of molybdenum (20 nm thick), titanium (20 nm thick), and nickel (10 nm thick). Both procedures yield similar nanofibers, but the addition of molybdenum and titanium films improve the electrical contact.

After deposition of the nickel, a brief initial treatment in a pure  $\text{NH}_3$  plasma was used to heat the sample and induce the nickel to dewet from the underlying substrate. The resulting nickel nanocrystals catalyze the growth of the VACNFs upon introduction of acetylene. Most nanofibers were grown in a flow of 100 standard cubic centimeters per minute (scm) ammonia and 36 scm acetylene at a total pressure of 4 Torr for a time ( $\sim 18$  min) sufficient to achieve a nanofiber length of  $1.0 \pm 0.3 \mu\text{m}$ . For experiments in which the edge-plane density of the VACNFs was varied,<sup>2</sup> three sets of growth parameters were used to generate nanofibers with varying internal structure. “Slow” VACNFs were grown using 200 scm  $\text{NH}_3$  and 85 scm  $\text{C}_2\text{H}_2$ , 5 Torr total pressure, and 1 A of current. “Medium” VACNFs were grown using 200 scm  $\text{NH}_3$  and 87 scm  $\text{C}_2\text{H}_2$ , 10 Torr total pressure, and 2 A of current. Finally, “fast” VACNFs were grown using 200 scm  $\text{NH}_3$  and 89 scm  $\text{C}_2\text{H}_2$ , 20 Torr total pressure, and 3 A of current. The growth continued for 20, 5, and 2 min respectively for slow, medium, and fast growths, such that the resulting nanofibers were  $\sim 2 \mu\text{m}$  tall.

To facilitate comparing the properties of VACNFs with those of more conventional nanostructured carbon materials, single-walled carbon nanotubes (SWCNTs) and multiwalled carbon nanotubes (MWCNTs) were grown in a low-pressure chemical vapor deposition benchtop system (Atomate) with an iron catalyst on  $\text{SiO}_2$ . The MWCNTs were grown with ethylene as a carbon source and argon as a diluent. The SWCNTs were grown in methane, hydrogen, and ethylene.

**Surface Functionalization.** The VACNFs were functionalized using a photochemical grafting procedure described previously<sup>7</sup> in which organic alkenes are linked to carbon surfaces using ultraviolet (UV) light at 254 nm. In the present work, we investigated three different alkenes with different terminal

- (18) Chen, P. H.; Fryling, M. A.; McCreery, R. L. *Anal. Chem.* **1995**, *67*, 3115.  
 (19) Chen, P. H.; McCreery, R. L. *Anal. Chem.* **1996**, *68*, 3958.  
 (20) Kim, T.; Lim, S.; Kwon, K.; Hong, S. H.; Qiao, W. M.; Rhee, C. K.; Yoon, S. H.; Mochida, I. *Langmuir* **2006**, *22*, 9086.  
 (21) Heng, L. Y.; Chou, A.; Yu, J.; Chen, Y.; Gooding, J. J. *Electrochem. Commun.* **2005**, *7*, 1457.  
 (22) Merkulov, V. I.; Hensley, D. K.; Melechko, A. V.; Guillorn, M. A.; Lowndes, D. H.; Simpson, M. L. *J. Phys. Chem. B* **2002**, *106*, 10570.  
 (23) Meyyappan, M.; Delzeit, L.; Cassell, A.; Hash, D. *Plasma Sources Sci. Technol.* **2003**, *12*, 205.  
 (24) Strother, T.; Knickerbocker, T.; Russell, J. N.; Butler, J. E.; Smith, L. M.; Hamers, R. J. *Langmuir* **2002**, *18*, 968.  
 (25) Nichols, B. M.; Butler, J. E.; Russell, J. N.; Hamers, R. J. *J. Phys. Chem. B* **2005**, *109*, 20938.  
 (26) Colavita, P. E.; Streifer, J. A.; Sun, B.; Wang, X. Y.; Warf, P.; Hamers, R. J. *J. Phys. Chem. C* **2008**, *112*, 5102.  
 (27) Colavita, P. E.; Sun, B.; Tse, K. Y.; Hamers, R. J. *J. Am. Chem. Soc.* **2007**, *129*, 13554.  
 (28) Lasseter, T. L.; Clare, B. H.; Abbott, N. L.; Hamers, R. J. *J. Am. Chem. Soc.* **2004**, *126*, 10220.  
 (29) Landis, E. C.; Hamers, R. J. *J. Phys. Chem. C* **2008**, *112*, 16910.  
 (30) Landis, E. C.; Hamers, R. J. *Chem. Mater.* **2009**, *21*, 724.  
 (31) Nichols, B. M.; Metz, K. M.; Tse, K. Y.; Butler, J. E.; Russell, J. N.; Hamers, R. J. *J. Phys. Chem. B* **2006**, *110*, 16535.

- (32) Chilkoti, A.; Ratner, B. D.; Briggs, D. *Chem. Mater.* **1991**, *3*, 51.  
 (33) Langley, L. A.; Villanueva, D. E.; Fairbrother, D. H. *Chem. Mater.* **2006**, *18*, 169.  
 (34) Langley, L. A.; Fairbrother, D. H. *Carbon* **2007**, *45*, 47.

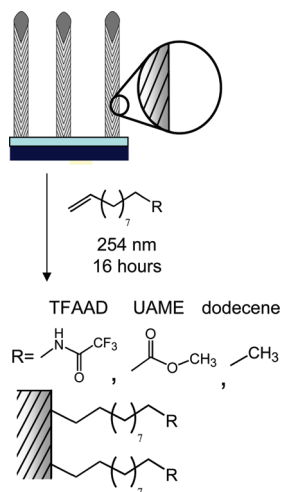


**Figure 1.** Reaction scheme of the photochemical functionalization on VACNFs.

groups depicted in Figure 1. Trifluoroacetic acid-protected 10-aminododec-1-ene (TFAAD) has been studied previously on diamond and other carbon surfaces.<sup>8,35–39</sup> TFAAD can be converted to a primary amine and used as a starting point for further linking of redox-active molecules and biomolecules to VACNF surfaces. It is the easiest of the three molecules to characterize, because of its distinct spectral signature in XPS.<sup>35</sup> Undecylenic acid methyl ester (UAME) is a precursor to carboxylic acid-modified VACNFs.<sup>7</sup> 1-Dodecene is a simple hydrocarbon with no additional functionality; functionalization with 1-dodecene leads to an extremely hydrophobic surface.

To graft these molecules to the VACNFs, a drop of the neat alkene (TFAAD, UAME, or dodecene) was placed on the VACNF sample and covered with a fused-silica window to prevent evaporation. This assembly was then illuminated with 254 nm light ( $\sim 10$  mW/cm<sup>2</sup>) from a low-pressure mercury lamp while purging with nitrogen; a duration of 16 h was typically used unless otherwise noted. After the reaction, samples were rinsed in alternating portions of methanol and chloroform.

**Surface Characterization.** Secondary electron images of the VACNF samples were obtained using a Hitachi Model S-4700 field-emission scanning electron microscopy (SEM) system. Imaging of the VACNF graphitic structure was achieved by high-resolution transmission electron microscopy (HRTEM), using a Hitachi HF-3300 cold field-emission microscope operated at 100 and 300 kV. Sample preparation for HRTEM analysis required the removal of the VACNFs from the substrate and their transfer to holey carbon-coated transmission electron microscopy (TEM) grids.

X-ray photoelectron spectroscopy (XPS) measurements were conducted in an ultrahigh-vacuum XPS system with a monochromatic Al K $\alpha$  source and a hemispherical analyzer with a 16-channel detector array. A 45° photoelectron takeoff angle was used for all spectra. Atomic area ratios for core-level spectra

were calculated by fitting the raw data to baseline-corrected Voigt functions and correcting the values using atomic sensitivity factors (C = 0.296, F = 1, O = 0.711).<sup>40</sup> Ultraviolet photoemission spectra (UPS) were obtained using a He(I) emission lamp (21.2 eV photon energy) and collected at 0.2 eV resolution with an electron takeoff angle of 45°. Samples were negatively biased to ensure that the vacuum level of the sample was higher in energy than the analyzer. Spectra were recorded at bias voltages sufficiently high that the high binding energy cutoff converged, and this value was used to calculate the work function.

Fourier transform infrared reflection–absorption spectroscopy (IRRAS) measurements were performed using a Fourier transform infrared spectrometer (Bruker Model Vertex70) with a variable-angle reflectance accessory (VeeMaxII, Pike). Spectra were collected using a 60° angle from the surface normal using *p*-polarized light at 4 cm<sup>−1</sup> resolution for both the background of unmodified nanofibers and the sample.

**Electrochemical Characterization.** Cyclic voltammetry measurements were performed using a three-electrode cell with an exposed area of 0.275 cm<sup>2</sup>. The carbon nanofiber samples were used as the working electrode with a platinum-mesh counter-electrode and a Ag/AgCl junctioned reference electrode. Cyclic voltammetry measurements were performed in 1 M KCl using the Ru(NH<sub>3</sub>)<sub>6</sub><sup>3+/2+</sup> and Fe(CN)<sub>6</sub><sup>3−/4−</sup> redox systems at concentrations of 4 mM. All solutions were made with water that was purified with a Nanopure filtration system (> 18 M $\Omega$  cm resistivity) and purged with argon before use.

**Oxide Group Derivatization.** Measurements of the distribution of oxidized sites on VACNFs were conducted using a method described by Langley and co-workers.<sup>33,34</sup> This method is based on highly selective reactions of certain fluorine-containing compounds with specific types of oxidized species, followed by XPS analysis to quantify the extent of reaction. Detailed procedures and controls are presented in the Supporting Information.

## Results

**X-ray and Ultraviolet Photoemission Spectroscopy.** To investigate the reactivity of VACNF surfaces, we used TFAAD as a model system. Figure 2a shows a survey spectrum of VACNFs before and after functionalization with TFAAD. Before functionalization, a large bulk carbon peak is visible at 283.7 eV. Smaller peaks from nitrogen and oxygen and from the nickel catalyst used in growth are also visible in the survey spectrum. The N peaks are attributed to substitutional nitrogen in the graphitic lattice, because of the ammonia used during growth.<sup>30</sup> After functionalization with TFAAD, XPS spectra show a new F peak and increases in the N and O peaks. The high-resolution carbon spectrum (Figure 2b) reveals a large peak at 283.7 eV, with higher-binding-energy C peaks at 292.2 and 288.1 eV. The C 1s peaks at higher binding energy can be attributed to specific C atoms from TFAAD. The peak at 292.2 eV arises from the −CF<sub>3</sub> group and the peak at 288.1 eV arises from the C=O group. The alkyl chain and the VACNFs both

- (35) Yang, W. S.; Auciello, O.; Butler, J. E.; Cai, W.; Carlisle, J. A.; Gerbi, J.; Gruen, D. M.; Knickerbocker, T.; Lasseter, T. L.; Russell, J. N.; Smith, L. M.; Hamers, R. J. *Nat. Mater.* **2002**, *1*, 253.
- (36) Hartl, A.; Schmich, E.; Garrido, J. A.; Hernando, J.; Catharino, S. C. R.; Walter, S.; Feulner, P.; Kromka, A.; Steinmüller, D.; Stutzmann, M. *Nat. Mater.* **2004**, *3*, 736.
- (37) Lu, M. C.; Knickerbocker, T.; Cai, W.; Yang, W. S.; Hamers, R. J.; Smith, L. M. *Biopolymers* **2004**, *73*, 606.
- (38) Nebel, C. E.; Shin, D.; Takeuchi, D.; Yamamoto, T.; Watanabe, H.; Nakamura, T. *Diamond Relat. Mater.* **2006**, *15*, 1107.
- (39) Nebel, C. E.; Shin, D.; Takeuchi, D.; Yamamoto, T.; Watanabe, H.; Nakamura, T. *Langmuir* **2006**, *22*, 5645.

- (40) Moulder, J. F.; Stickle, W. F.; Sobol, P. E.; Bomben, K. D. *Handbook of X-ray Photoelectron Spectroscopy*; Perkin–Elmer Corp.: Eden Prairie, MN, 1992.

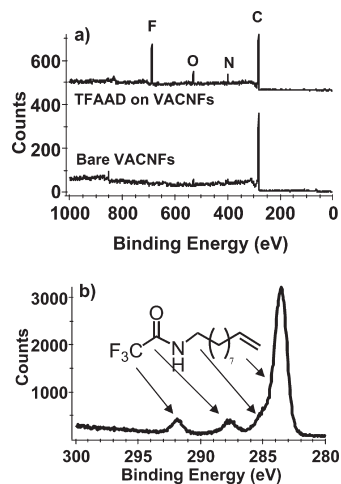


**Figure 2.** XPS spectra of TFAAD reacted with VACNF surface for 16 h: (a) survey spectrum showing bare and functionalized surfaces, and (b) C 1s region after TFAAD attachment, showing high-binding-energy C peaks.

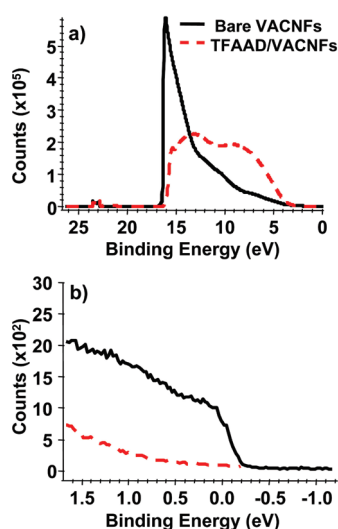


**Figure 3.** UPS spectra of (a) bare and TFAAD-functionalized VACNF surfaces, and (b) the low-energy region of bare and functionalized VACNFs, showing the Fermi step.

contribute to the bulk carbon peak at 284 eV. These features are all similar to those reported previously.<sup>35,41</sup>

The as-grown VACNFs and TFAAD functionalized samples were also characterized using He(I) ultraviolet photoemission spectroscopy (UPS) before and after functionalization. Figure 3a shows the full spectra, whereas Figure 3b shows an expanded view of the region near the Fermi energy ( $E_F = 0$  eV). The bare VACNFs yield a single broad peak with a maximum at 16.1 eV and weaker features near 11 and 7 eV. These features can be assigned based on previous work on graphite.<sup>42</sup> The peak at 16 eV is attributed to an s-like  $\sigma$ -band. The intensity near 7 eV arises from  $p\sigma$ -bands, while the intensity at smaller binding energies is the result of  $p\pi$ -bands. These features are

very similar to those reported previously on graphite and glassy carbon.<sup>42</sup>

Because our previous work showed that grafting was induced by an internal photoemission process (i.e., excitation from the valence band of the substrate to a molecular acceptor level), we measured the work function of bare VACNFs by finding the energy of the high-binding-energy cutoff and subtracting this from the incident photon energy of 21.2 eV. The resulting value of 4.79 eV is slightly smaller than the photon energy (4.88 eV) used in grafting. Figure 3b shows that the bare nanofibers exhibit a sharp Fermi edge. This sharp edge demonstrates that the nanofibers are metallic, with a significant density of states near the Fermi energy. Spectra obtained on nanofibers grown at different rates (see the Supporting Information) showed no significant differences in the UPS spectra; all three samples showed a Fermi edge of roughly comparable shape, allowing us to conclude that nanofibers grown at different rates have similar valence electronic structures.

Photochemical grafting of TFAAD to the VACNF surface produced notable changes in the UPS spectra. Small local maxima are visible at 15.4 eV and 13.1 eV, with a broad peak at  $\sim 9$  eV. Previous UPS studies of solid-phase alkanes show that the peak at 13 eV arises from the C 2s band, while the peak at  $\sim 9$  eV arises from the C 2p band.<sup>43</sup> On the TFAAD functionalized samples, the Fermi step is significantly attenuated. While this attenuation could suggest that grafting reduces the Fermi level density of states, electrons emitted from near the Fermi energy (kinetic energy of  $\sim 21$  eV) have an inelastic mean free path of only  $\sim 1$  nm,<sup>44</sup> comparable to the length of the molecules being grafted. Thus, the low emission intensity near zero binding energy is largely a consequence of inelastic scattering in the molecular layer; this is further supported by electrochemical measurements (vide infra), showing good electrochemical activity after functionalization. Measurements of UPS spectra near the high binding energy cutoff show that functionalization increases the work function very slightly, to 5.16 eV.

**Rate of Grafting and Dependence on Molecular Structure.** The overall rate of TFAAD grafting was measured using XPS to characterize the F:C ratio. Figure 4a shows the ratio of the F 1s and C 1s peak areas ( $A_{F(1s)}/A_{C(1s)}$ ) after correcting for the appropriate sensitivity factors. The F:C ratio increases linearly for the first 16 h of the reaction before reaching a constant value of 0.26. Because of the complex geometry of the nanofiber sample, it is difficult to relate this number to an absolute coverage. However, at long times, the data suggest that the reaction either self-terminates, because of saturation of available surface sites, or reaches a constant composition, because of multilayer formation. Electrochemical data (vide infra) showing that the majority of the nanofiber surface is electrochemically active after functionalization suggest the former.

(41) Sun, B.; Colavita, P. E.; Kim, H.; Lockett, M.; Marcus, M. S.; Smith, L. M.; Hamers, R. J. *Langmuir* **2006**, *22*, 9598.

(42) McFeely, F. R.; Kowalczyk, S. P.; Ley, L.; Cavell, R. G.; Pollak, R. A.; Shirley, D. A. *Phys. Rev. B* **1974**, *9*, 5268.

(43) Pireaux, J. J.; Caudano, R. *Phys. Rev. B* **1977**, *15*, 2242.

(44) Seah, M. P.; Dench, W. A. *Surf. Interface Anal.* **1979**, *1*, 2.

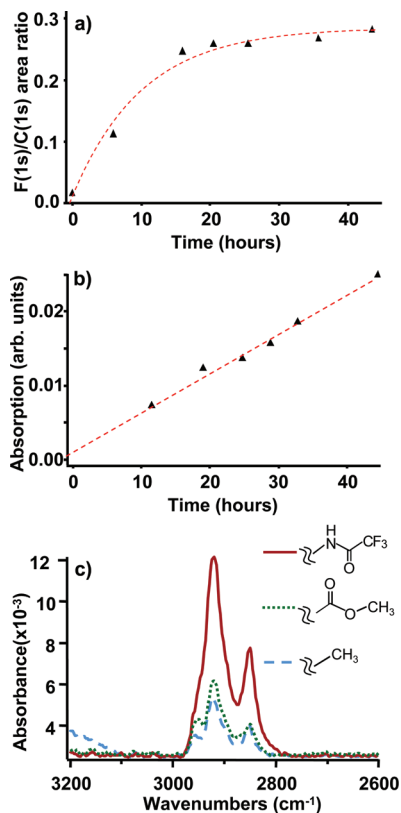


**Figure 4.** (a) Kinetic curve of TFAAD functionalization on the VACNF surface with TFAAD coverage calculated from F1s/C1s XPS ratios; (b) kinetic curve of UAME functionalization on VACNF surface obtained using CH<sub>2</sub> infrared absorption; and (c) IRRAS of the CH<sub>2</sub> region after 16 h photochemical reactions with dodecane, UAME, or TFAAD. The varying molecular density is apparent from the differences in peak intensity.

The rate of reaction of other molecules cannot be assessed easily using XPS, because of the absence of robust spectral signatures of the molecules. Therefore, we used FTIR spectra to compare the grafting of TFAAD, UAME, and 1-dodecene onto VACNFs, using the integrated intensity of the CH<sub>2</sub> stretching region. UAME does not graft as quickly as TFAAD, and Figure 4b shows that with UAME the reaction rate inferred from FTIR measurements is linear with time and that the reaction has not yet self-terminated at the longest times used. Figure 4c shows the CH<sub>2</sub> region of all three samples illuminated for 16 h, showing that, under these conditions, TFAAD has the largest CH infrared absorbance, UAME has less, and 1-dodecene has the least. Because the VACNF substrates used in these studies are otherwise identical and all three molecules have similar lengths, we attribute these differences in CH<sub>2</sub> infrared absorbance to differences in surface coverage that arise from the different rates at which each molecule grafts: TFAAD grafts most quickly, UAME more slowly, and 1-dodecene the slowest. Based on these and other similar FTIR spectra, we chose 16 h as a standard time at which to compare the properties of the photochemically modified VACNF samples. This time was chosen because it corresponds to the time at which the fastest-grafting molecule (TFAAD) approaches its terminal F1s:C1s

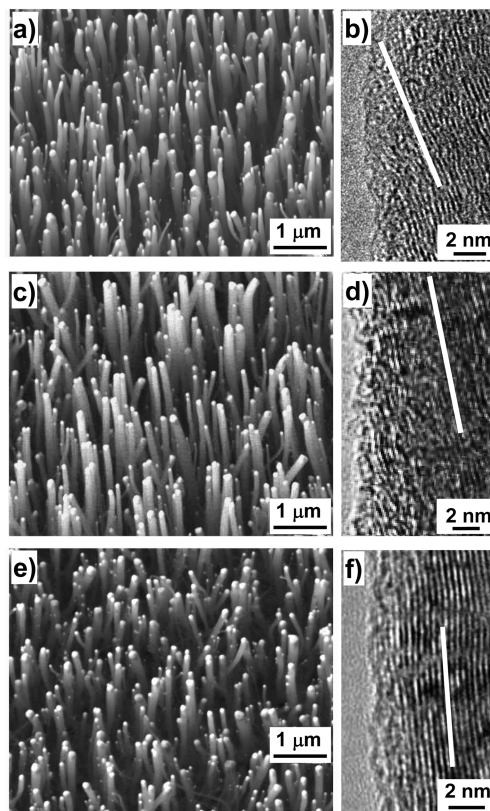


**Figure 5.** Electron microscopy images of VACNFs grown with varying amounts of edge-plane graphite: (a, c, e) SEM images of VACNFs grown under slow, medium, and fast rates, respectively; (b, d, f) TEM images of VACNFs grown under slow, medium, and fast rates, respectively, showing that the graphene planes intersect the nanofiber sidewalls (the white bar is parallel to the graphene sheets and is intended only to guide the eye).

XPS ratio. Because the FTIR data show that the other molecules graft more slowly than TFAAD, this allows us to compare reactivity under conditions where any possibility of multilayer formation is negligible.

**The Role of Edge-Plane Density.** In previous work,<sup>29,30</sup> we proposed that photochemical grafting of alkenes might proceed preferentially at the edge-plane sites. To determine whether the amount of edge-plane graphite along the nanofiber sidewalls has a significant effect on the density of grafted molecules, we grew nanofibers with different amounts of exposed edge-plane sites, as described previously. In previous work,<sup>2</sup> we showed that increasing the total pressure during growth leads to nanofibers in which the graphitic planes are more nearly parallel to the nanofiber sidewalls, thereby decreasing the amount of edge-plane sites exposed along the nanofiber sidewalls. Figure 5 shows SEM images (Figures 5a, c, e) and TEM (Figures 5b, d, f) images of nanofiber samples grown at three different growth rates. To facilitate direct comparison, we adjusted the growth time so that all nanofibers had a similar length of ~2 μm. SEM images show similar diameters and densities for fibers grown at slow (Figure 5a), medium (Figure 5b), and fast (Figure 5c) growth rates. However, TEM images show distinct differences in the angle at which the graphene sheets intersect the nanofiber sidewalls, resulting in different amounts of edge-plane sites exposed, with the slowest

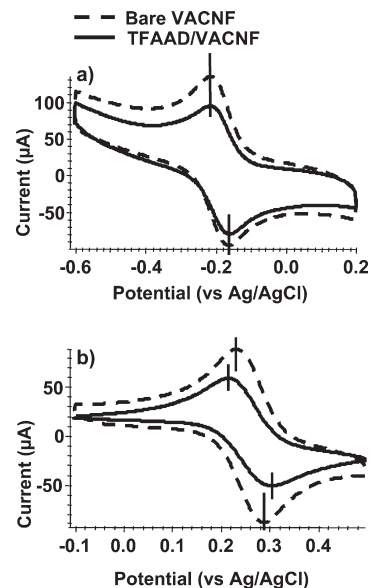
**Table 1.** XPS Area Ratios of VACNFs Grown at Different Rates after Grafting with TFAAD

growth	Area Ratio		
	F:C	N:C	O:C
fast	0.157 ± 0.004	0.062 ± 0.008	0.062 ± 0.015
medium	0.167 ± 0.003	0.081 ± 0.008	0.072 ± 0.02
slow	0.252 ± 0.003	0.087 ± 0.002	0.078 ± 0.02

growth (Figure 5b) showing the largest angle and the medium growth (Figure 5d) and especially the fast growth (Figure 5f) showing planes intersecting at shallower angles. The white bars in Figures 5b, d, and 5f show representative measurements of the orientation of the graphene sheets. We analyzed numerous TEM images from each sample to determine the average spacing between exposed edge-plane sites along the VACNF sidewalls. The slowest growth leads to the smallest separation (of  $9.7 \pm 0.8 \text{ \AA}$ ) between edge-plane sites, whereas the fastest growth produced a substantially larger separation ( $\sim 27 \text{ \AA}$ ) between edge-planes. The medium growth rate produced an intermediate separation of  $\sim 13 \text{ \AA}$  between edge-plane sites. Because the nanofiber diameter is controlled by the nickel catalyst, the nanofibers grown by the three methods have the same average diameter of 70 nm.

To characterize how the differences in edge-plane graphite affected photochemical grafting, XPS measurements were performed on the VACNFs functionalized with TFAAD. Table 1 shows the resulting peak area ratios  $A_{F(1s)}/A_{C(1s)}$ ,  $A_{N(1s)}/A_{C(1s)}$ , and  $A_{O(1s)}/A_{C(1s)}$ . The F:C ratios are a good way to assess the surface binding density, because the bare nanofibers lack fluorine. The nanofibers with the lowest density of exposed edge-plane sites had a F:C ratio of  $0.157 \pm 0.004$ , while the nanofibers with intermediate edge-plane density had a slightly higher ratio of  $0.167 \pm 0.003$ , and the nanofibers with the highest density of edge-plane graphite had a F:C ratio of  $0.252 \pm 0.003$ . The N:C and O:C ratios are less useful for quantification, because the as-grown nanofibers have nitrogen from the  $\text{NH}_3$  source gas<sup>30</sup> and may have oxygen in the bulk or from water adsorbed onto the surface. However, for the functionalized fibers, the amount of nitrogen and oxygen increases as the spacing between exposed edge-plane sites decreases. Thus, our XPS data clearly show that controlling the growth to yield a higher density of edge-plane sites also increases the number of molecules grafted to the surface.

**Electrochemical Probes of Nanofiber Structure and Electron-Transfer Properties.** Previous studies have shown that certain redox-active species can be used to probe for different types of species at carbon electrodes. For example, the electron-transfer kinetics of the  $\text{Fe}(\text{CN})_6^{3-/4-}$  redox couple are very sensitive to the amount of edge-plane graphite on a surface.<sup>17</sup> In contrast, the  $\text{Ru}(\text{NH}_3)_6^{3+/2+}$  redox couple is relatively insensitive to the presence of oxidized groups or other surface groups, and its electron-transfer kinetics are determined by the Fermi-level density of states of the electrode material.<sup>18,19</sup> We used these two probes to provide more insight into the

**Figure 6.** Cyclic voltammogram obtained on bare and TFAAD-functionalized VACNFs using the (a)  $\text{Ru}(\text{NH}_3)_6^{3+/2+}$  and (b)  $\text{Fe}(\text{CN})_6^{3-/4-}$  redox couples.

types of structures present at the VACNF sidewalls, yielding the results shown in Figure 6. The splitting between the peak in the oxidation and reduction waves can be used to characterize the rate of electron transfer, with faster electron transfer leading to a smaller peak-to-peak separation.<sup>45</sup> When using the  $\text{Ru}(\text{NH}_3)_6^{3+/2+}$  redox couple (Figure 6a), the bare (as-grown) VACNFs yield a peak to peak splitting  $\Delta E_p = 67 \pm 2 \text{ mV}$ . After functionalization with TFAAD for 16 h, the peak-to-peak splitting was  $66 \pm 3 \text{ mV}$ , essentially unchanged. There is also a slight reduction in the peak current. This similarity indicates that the overall Fermi-level density of states of the nanofibers is not significantly impacted by the photochemical functionalization, but the molecular layer does slightly reduce the available redox-active area. When using the  $\text{Fe}(\text{CN})_6^{3-/4-}$  redox couple, however, more significant differences emerge. While the bare nanofibers yield a peak-to-peak splitting of  $58 \pm 5 \text{ mV}$ , after grafting of TFAAD, the splitting increases to  $76 \pm 3 \text{ mV}$  and the peak current is reduced to approximately half its original value. The fact that photochemical grafting substantially increases the  $\text{Fe}(\text{CN})_6^{3-/4-}$  peak-to-peak splitting while leaving the  $\text{Ru}(\text{NH}_3)_6^{3+/2+}$  splitting unchanged indicates that photochemical functionalization with TFAAD decreases the amount of electrochemically active edge-plane sites but leaves a significant amount of basal-plane graphite exposed and electrochemically accessible.

To characterize how molecular grafting impacts the electrochemical properties of the electrodes, we again utilized the  $\text{Ru}(\text{NH}_3)_6^{3+/2+}$  and  $\text{Fe}(\text{CN})_6^{3-/4-}$  redox-active probes after grafting of the alkenes to the VACNFs for 16 h. Table 2 summarizes the results. When using  $\text{Ru}(\text{NH}_3)_6^{3+/2+}$ , the three functionalized surfaces and the bare surface show almost identical peak separations, demonstrating that none of the functionalization molecules

(45) Nicholson, R. S. *Anal. Chem.* **1965**, *37*, 1351.

**Table 2. Electrochemical Data on Bare and Covalently Functionalized VACNFs**

surface	Peak-to-Peak Splitting (mV)		capacitance in 1 M KCl (mF/cm <sup>2</sup> )
	Ru(NH <sub>3</sub> ) <sub>6</sub> <sup>3+/2+</sup>	Fe(CN) <sub>6</sub> <sup>3-/4-</sup>	
bare	67 ± 2	58 ± 5	1.13 ± 0.16
1-dodecene	67 ± 1	66 ± 1	NA
UAME	63 ± 3	74 ± 5	1.05 ± 0.07
TFAAD	66 ± 3	76 ± 3	0.96 ± 0.16

significantly change the electronic nature of the underlying VACNF substrates. However, much more significant changes are observed when using the Fe(CN)<sub>6</sub><sup>3-/4-</sup> redox couple, which is sensitive to the amount of edge-plane graphite.<sup>17</sup> On the bare VACNF surface, the Fe(CN)<sub>6</sub><sup>3-/4-</sup> redox couple yields a peak-to-peak splitting of 58 ± 5 mV. When dodecene, which is the least reactive molecule, was attached to the surface, the peak-to-peak splitting increased to 66 mV; the 8 mV increase in splitting is outside the margin of experimental error. Even larger splittings result from grafting of the methyl ester (74 ± 5 mV) or TFAAD (76 ± 3 mV) onto the surface. Because our infrared data (Figure 4c) show that the trend in number density of grafted molecules is 1-dodecene < UAME < TFAAD, our electrochemical data again suggest that all three molecules preferentially bind to the graphitic edge-plane sites, and that the differences in electrochemical behavior after grafting of the three molecules are primarily a result of the different number density of molecules that graft under these conditions.

As another independent test of the electrically accessible area, we investigated how molecular grafting influenced the interfacial capacitance of the VACNFs in 1 M KCl solutions. The capacitance was measured at potentials near the open circuit potential, where the current was independent of voltage, signifying the absence of any Faradaic processes. As shown in Table 2, these measurements show a small decrease in the capacitance due to grafting of molecules to the VACNFs. The bare nanofibers had a capacitance of 1.13 ± 0.16 mF/cm<sup>2</sup>, whereas those functionalized with TFAAD had a capacitance of 0.96 ± 0.16 mF/cm<sup>2</sup>. The UME functionalized surface fell between the two extremes, at 1.05 ± 0.07 mF/cm<sup>2</sup>. It was not possible to measure the dodecene functionalized surfaces, because they do not wet. The above results for TFAAD and UAME show that grafting occurs selectively at the edge-plane sites exposed along the nanofiber sidewalls. Grafting does not significantly impede electron-transfer processes of the “inner-sphere” couple Ru(NH<sub>3</sub>)<sub>6</sub><sup>3+/2+</sup>, whereas the outer-sphere couple Fe(CN)<sub>6</sub><sup>3-/4-</sup> is strongly affected. This is consistent with previous studies on graphite,<sup>46</sup> which found that Fe(CN)<sub>6</sub><sup>3-/4-</sup> requires special surface sites for facile electron transfer. Our results imply that grafting leaves the basal plane sites exposed where they remain accessible for redox reactions; the exposed basal plane sites also support an ionic double-layer immediately adjacent to the electrode

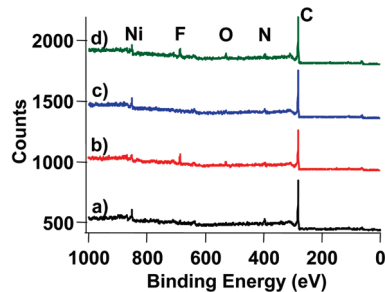


**Figure 7.** XPS survey spectrum of VACNFs showing the results of selective fluorination with trifluoroacetic acid: (a) bare VACNFs, (b) bare VACNFs derivatized with trifluoroacetic acid, (c) dodecene-functionalized VACNFs, and (d) dodecene-functionalized VACNFs derivatized with trifluoroacetic acid.

surface without an intervening molecular layer, resulting in a high capacitance even after grafting.

**Influence of Oxidized Surface Sites.** Because surface oxygen can play a role in electrochemical properties of carbon,<sup>46,47</sup> we used the method developed by Langley and co-workers<sup>33,34</sup> to identify the relative amounts of different oxygen-containing groups on VACNF samples. This method uses highly selective derivatization reactions between fluorinated compounds and specific types of surface oxidized sites, followed by the use of XPS to quantify the amount of fluorine present after derivatization. Detailed procedures and control experiments are described in the Supporting Information. To illustrate the method, Figure 7 shows a sample XPS survey spectrum of a VACNF sample after derivatization with trifluoroacetic acid, which selectively reacts with –OH groups. Before functionalization, Figure 7a shows that spectra of bare VACNFs exhibit a large bulk carbon peak at 281.6 eV, a smaller O 1s peak at 539.7 eV, N 1s peaks at 398.2 and 396.0 eV, and a peak from nickel at 851.5 eV that arises from the catalyst used during growth. No significant fluorine was observed on the bare VACNF samples. Figure 7b shows a spectrum after derivatization with trifluoroacetic acid; this spectrum shows C 1s, O 1s, and N 1s peaks that are similar to those of the underivatized sample, but with a new F 1s peak that is due to reaction with surface –OH groups. Similarly, Figure 7c shows a survey spectrum of dodecene-modified VACNFs, whereas Figure 7d shows the spectrum after the –OH groups of the dodecene-modified sample were derivatized with trifluoroacetic acid. Quantitative analysis of high-resolution spectra (not shown) establishes that surface –OH groups accounted for 29.8% ± 1.3% of all oxygen on the “bare” VACNFs and 32% ± 4% of all oxygen after the grafting of 1-dodecene; these values are indistinguishable (within experimental error).

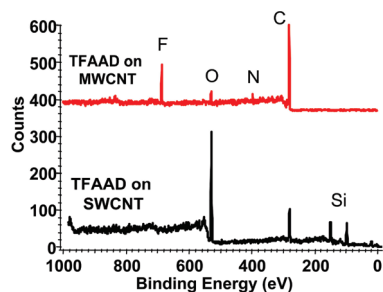
Similar experiments were conducted using other derivatizing agents that previous studies<sup>33,34</sup> have shown to be selective for carboxylic acid groups and for carbonyl groups, as described in the Supporting Information. The results of these derivatization experiments are summarized in Table 3. Overall, the results for surface –OH

(46) Cline, K. K.; McDermott, M. T.; McCreery, R. L. *J. Phys. Chem.* **1994**, *98*, 5314.

(47) McCreery, R. L.; Cline, K. K.; McDermott, C. A.; McDermott, M. T. *Colloids Surf. A* **1994**, *93*, 211.

**Table 3. Oxidized Forms of Carbon on VACNFs before and after Grafting of 1-Dodecene, Identified Using a Selective Derivatization Method**

	%OH	%COOH	%COCH <sub>3</sub>
bare VACNFs	29.8 ± 1.3	17 ± 3	29 ± 11
dodecene-functionalized VACNFs	32 ± 4	14 ± 4	15 ± 5

**Figure 8.** XPS survey spectrum of MWCNT and SWCNT reacted with TFAAD for 16 h. (The SWCNT spectrum was shifted to correct for charging.)

groups, carboxylic acids, and carbonyl groups all show that there is no statistically significant change in composition induced by photochemical grafting of alkenes to the VACNF surfaces. Thus, we conclude that, although surface oxides are undoubtedly present and may indirectly affect the grafting kinetics, the oxide functional groups are not significantly altered by the photochemical grafting of alkenes onto VACNFs. Similarly, we conclude that the effects of grafting on the electrochemical properties are not due to changes in surface oxides, but instead are a direct consequence of the molecular grafting.

**Control Samples of Single-Walled and Multiwalled Carbon Nanotubes.** To further test the differences in reactivity of edge-plane and basal-plane sites, we conducted experiments on single-walled carbon nanotubes (SWCNTs) and multiwalled carbon nanotubes (MWCNTs). Because SWCNTs expose edge-plane graphite only at their ends and at defect sites, we hypothesized that grafting would not occur on the SWCNTs. As shown in Figure 8, SWCNTs that were exposed to TFAAD and illuminated for 16 h showed no measurable fluorine peak in XPS. Using the XPS noise level in the F 1s region, we determined that the detection limit for fluorine would correspond to a peak area ratio of  $A_{F(1s)}/A_{C(1s)} = 0.019$ . In comparison with the values of 0.16–0.25 observed on VACNFs, we conclude that the grafting reaction is at least 10 times less efficient on SWCNTs than on VACNFs.

Additional control experiments were performed using MWCNTs; XPS measurements after grafting of TFAAD yielded an area ratio of  $A_{F(1s)}/A_{C(1s)} = 0.20$ , which is comparable to the values observed for VACNFs. To confirm whether the grafting on MWCNTs was due to the presence of exposed graphitic edge-planes, the electrochemical properties of the as-grown MWCNT samples were investigated with the  $Ru(NH_3)_6^{3+/2+}$  and  $Fe(CN)_6^{3-/4-}$  redox-active probes. The peak-to-peak splitting using  $Ru(NH_3)_6^{3+/2+}$  was  $56 \pm 3$  mV, which is lower than the value of  $67 \pm 2$  mV observed on the VACNF surfaces. Measurements using the  $Fe(CN)_6^{3-/4-}$  redox

couple (which is sensitive to edge-plane graphite) yielded peak-to-peak splitting of  $63 \pm 5$  mV on the MWCNTs, compared with  $58 \pm 5$  mV on bare VACNFs. The larger splitting with  $Fe(CN)_6^{3-/4-}$  on MWCNTs indicates that the MWCNTs have a lower density of edge-plane graphite than the bare VACNFs, despite having a larger overall accessible area.

## Discussion

While the electronic properties of edge-plane and basal-plane graphite are well-known,<sup>15,17,47–49</sup> much less is known about how edge-plane sites influence grafting of molecules to the surface.<sup>50</sup> It is generally recognized that the edge-plane sites exhibit much-higher electron-transfer rates,<sup>17</sup> and studies of nanotubes have established that edge-plane sites at the nanotube ends and at wall defects are responsible for their electrocatalytic activity.<sup>14,15,51,52</sup> Indeed, in many cases, mechanical or harsh chemical methods are used to intentionally disrupt the perfect graphitic structure, increase the exposed edge-plane sites, and enhance the electron-transfer characteristics.<sup>21</sup> Although these studies have demonstrated the importance of exposed edge-planes, the influence of edge-plane versus basal-plane graphite on photochemical grafting reactions has not been investigated previously. Our studies provide several new insights into photochemical grafting onto VACNFs and the resulting impact on electrochemical properties. These factors ultimately control whether molecular layers can be used advantageously to control the selectivity and electrochemical performance of VACNFs.

### Role of Edge-Plane Graphite in Photochemical Grafting.

The data in Table 1 show that the density of molecules grafted to the VACNFs increases commensurate with the amount of edge-plane graphite exposed along the side-walls. Grafting is less efficient on multiwalled nanotubes and is undetectable on single-walled nanotubes, which is consistent with the trends in edge-plane graphite detected electrochemically using the  $Fe(CN)_6^{3-/4-}$  redox couple. These results show that edge-plane graphite sites play an essential role in the photochemical grafting on VACNFs and likely on other nanostructured carbons as well.

The correlation between edge-plane density and grafting efficiency alone does not establish whether the role of the edge-plane sites is to improve initiation of the reaction or if edge sites are the actual grafting locations on the surface. However, the measurements showing that the photochemical grafting of molecules to the VACNFs affects the electron-transfer kinetics of  $Fe(CN)_6^{3-/4-}$  (which is sensitive to edge-plane graphite) but does not

(48) McDermott, M. T.; Kneten, K.; McCreery, R. L. *J. Phys. Chem.* **1992**, *96*, 3124.

(49) McCreery, R. L. *Chem. Rev.* **2008**, *108*, 2646.

(50) Klein, K. L.; Melechko, A. V.; McKnight, T. E.; Retterer, S. T.; Rack, P. D.; Fowlkes, J. D.; Joy, D. C.; Simpson, M. L. *J. Appl. Phys.* **2008**, *103*.

(51) Banks, C. E.; Moore, R. R.; Davies, T. J.; Compton, R. G. *Chem. Commun.* **2004**, 1804.

(52) Gong, K. P.; Chakrabarti, S.; Dai, L. M. *Angew. Chem., Int. Ed.* **2008**, *47*, 5446.

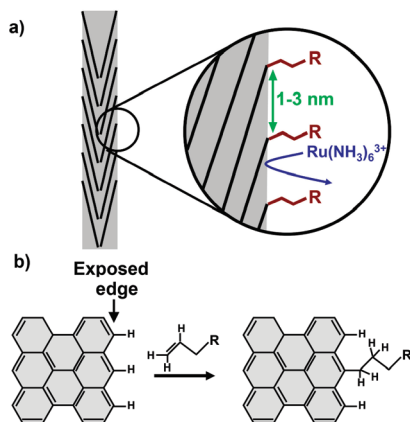


**Figure 9.** Schematic illustrations of functionalized nanofibers: (a) illustration of VACNF structure after selective grafting of alkenes to nanofiber step edges and (b) one possible reaction pathway for grafting alkenes to H-terminated edge plane sites on nanofiber sidewalls. Other pathways are also possible.

significantly impact the kinetics of the  $\text{Ru}(\text{NH}_3)_6^{3+/2+}$  couple implies that the grafting occurs selectively at the edge-plane sites. Figure 9a depicts the overall structure that can be achieved; our results suggest that the separation between step edges can be easily adjusted over the range of  $\sim 1\text{--}3$  nm.

To understand *why* molecules preferentially link to the step edges, we note that, in previous studies of photochemical grafting of alkenes on diamond and amorphous carbon, we established that grafting was initiated by photoemission of electrons from the sample into acceptor states of the adjacent alkene.<sup>25–27,53</sup> Those experiments showed that the reactivity was strongly correlated with the electron affinity of the reactant molecules, and that TFAAD was exceptionally reactive because the trifluoroacetamide group is an especially good electron acceptor.<sup>27</sup> However, recent studies have shown that the spatial location of molecules grafting to diamond is not controlled by the photoemission site, but rather by the *holes* that are left behind. In this mechanism, photoemission of electrons into alkenes (strongly dependent on the molecular electron affinity) creates “persistent” holes in the substrate that then serve as reactive sites for nucleophilic addition by the electron-rich vinyl group of the reactant olefins.<sup>27,54</sup> The trends in reactivity between the molecules investigated here (see Figure 4c) are consistent with the trends in reactivity and in electron affinity identified in previous studies on diamond and amorphous carbon.<sup>27,53</sup> Since our experiments use UV photons whose energy (4.88 eV) exceeds that of the work function of the nanofibers under vacuum (4.75 eV), we believe that a similar mechanism is likely active on VACNFs.

To explain why the molecules preferentially bond at the step edges, we note that previous studies of large polycyclic aromatic hydrocarbons have found that their cations have the positive charge localized on the C atoms at the edges,<sup>55</sup> which suggests that these should be unusually

reactive sites for reaction with electron-rich olefin ( $\text{C}=\text{C}$ ) groups. The density of states near the Fermi energy can be increased by the introduction of disorder into graphite,<sup>46</sup> and studies of graphite and graphenes show that there is a localized state at the Fermi level associated with “zig-zag” graphitic edges.<sup>56–58</sup> These studies suggest that graphitic edge sites would likely be an excellent site for trapping holes, thereby facilitating preferential reaction of the alkenes at the edge-plane sites. Figure 9a depicts one possible pathway, assuming an exposed edge of the zigzag structure and assuming that the unsaturated bonds at the edge are terminated with H atoms because of the hydrogen-rich environment during nanofiber growth.

**Impact of Molecular Grafting on Electrochemical Properties.** One motivation for these studies has been to understand how to optimize the use of molecular layers as integral components of inorganic–organic hybrid materials for applications such as electrocatalysis or sensing, where molecular layers are used to confer specific properties such as chemical or biological selectivity, but where the electron-transfer properties are also of interest. Our results show that grafting of molecules to the graphite edge planes significantly impedes the electron-transfer properties of the  $\text{Fe}(\text{CN})_6^{3-/4-}$  couple, yet, the peak-to-peak splitting of the  $\text{Ru}(\text{NH}_3)_6^{3+/2+}$  redox couple does not change significantly; and the peak redox current, using both couples, changes by a factor of  $< 2$ . Furthermore, the interfacial capacitance measurements show only a 16% decrease in capacitance after functionalization (from  $1.14\text{ mF/cm}^2$  to  $0.96\text{ mF/cm}^2$ ) for the molecule with the highest grafting efficiency (TFAAD).<sup>29</sup> If the molecular layers formed a continuous layer, then they would be expected to introduce a new series capacitance that would reduce the total capacitance. For example, studies on a gold surface with molecular layers of similar length revealed much more pronounced decreases in capacitance, by a factor of 6 or more.<sup>59,60</sup> Our results show that the photochemical grafting occurs only at the edge-plane sites, leaving the basal plane sites exposed, as depicted in Figure 9a.

Ultimately, designing an optimum electrode structure for processes such as electrocatalysis or sensing requires control of the density of surface-linked functionalities (e.g., electrocatalytic centers, biomolecular binding sites) and the electron-transfer properties. For many applications, it is advantageous to have a molecular layer that is *permeable* to redox species. Our results show that the properties can be controlled by tuning the number density of step-edge sites exposed along the nanofiber sidewall.

## Conclusions

Our results show that photochemical grafting of molecules onto vertically aligned carbon nanofibers occurs

(53) Colavita, P. E.; Sun, B.; Wang, X. Y.; Hamers, R. J. *J. Phys. Chem. C* **2009**, *113*, 1526.

(54) Wang, X.; Colavita, P. E.; Streifer, J. A.; Butler, J. E.; Hamers, R. J. Submitted to *J. Phys. Chem. C*, **2009**.

(55) Pathak, A.; Rastogi, S. *Chem. Phys.* **2006**, *326*, 315.

(56) Giunta, P. L.; Kely, S. P. *J. Chem. Phys.* **2001**, *114*, 1807.

(57) Fujita, M.; Wakabayashi, K.; Nakada, K.; Kusakabe, K. *J. Phys. Soc. Jpn.* **1996**, *65*, 1920.

(58) Kobayashi, Y.; Fukui, K.; Enoki, T.; Kusakabe, K. *Phys. Rev. B* **2006**, *73*, 125415.

(59) Miller, C.; Cuendet, P.; Gratzel, M. *J. Phys. Chem.* **1991**, *95*, 877.

(60) Widrig, C. A.; Chung, C.; Porter, M. D. *J. Electroanal. Chem.* **1991**, *310*, 335.

selectively at the exposed edge-plane sites and likely occurs via a photoemission-initiated process similar to that reported previously on diamond. The exposed basal plane sites remain electrochemically accessible to inner-sphere redox probes such as  $\text{Ru}(\text{NH}_3)_6^{3+/2+}$ . By varying the nanofiber growth conditions, it is possible to tune the amount of edge-plane graphite and thereby control the ratio of edge-plane to basal-plane sites. This connection between surface structure and chemical reactivity indicates that the chemical functionalization of the surfaces can be controlled through both chemical means and through the underlying surface structure. These results may yield the ability to make redox-active electrodes with enhanced selectivity and good redox properties for applications such as electrocatalysis and sensing.

**Acknowledgment.** This work was supported in part by the National Science Foundation (Grant Nos. DMR0706559 and CHE0911543). K.L.K. and D.K.H acknowledge support from the Center for Nanophase Materials Sciences. A. V.M. acknowledges support from the Division of Materials Sciences and Engineering of the DOE Office of Science. A portion of this research was conducted at the Center for Nanophase Materials Science, which is sponsored at Oak Ridge National Laboratory by the Scientific User Facilities Division, Office of Basic Energy Sciences, U.S. Department of Energy, via CNMS Project CNMS2007-252.

**Supporting Information Available:** Ultraviolet photoemission spectra of nanofibers synthesized at different growth rates. Detailed procedures and controls for analysis of oxidized surface sites via derivatization reactions. (PDF) This information is available free of charge via the Internet at <http://pubs.acs.org/>.